Chapter 7

Goal-equivalent variability explained by interhemispheric interactions

7.1 Introduction

Goal-equivalent variability is a dominant feature of human movements. In Chapter 4 , our experimental study of a coordinated bimanual task demonstrated a correlation between cortical activity and goal-equivalent variability in output forces (Babikian et al. 2017). Our head maps of cortical activity showed that trial-to-trial variability may therefore be produced, at least partly, by cortical signals in the primary motor cortices (Figure 4.3).

The hand area of the primary motor cortex (M1) controls hand movements and force productions. Coordinated bimanual tasks, such as that we used in our experimental study, rely heavily on callosally mediated communication (Carson 2005, Fling & Seidler 2012), i.e., neural interactions between the left and right hemispheres. These interhemispheric interactions may consist of facilitatory (excitatory) and/or inhibitory connections. At the level of the primary motor cortices, the interaction is primarily inhibitory, i.e., there is mutual inhibition between the two M1s (Ferbert, Priori, Rothwell, Day, Colebatch &

Marsden 1992, Kujirai, Caramia, Rothwell, Day, Thompson, Ferbert, Wroe, Asselman & Marsden 1993, Grefkes, Eickhoff, Nowak, Dafotakis & Fink 2008). This interhemispheric inhibition helps prevent interference of control processes between the two opposing cortices (Fling, Peltier, Bo, Welsh & Seidler 2011).

Interhemispheric interactions have been well-studied using Transcranial Magnetic Stimulation (TMS) (Ferbert et al. 1992, Kobayashi & Pascual-Leone 2003), a non-invasive procedure that directly but non-invasively stimulates nerve cells in the brain using magnetic fields. In studies exploring interhemispheric interactions at the level of the hand, a first stimulus, called the "conditioning stimulus" is sent to one of the M1s, and a second "test stimulus" is sent to the opposing M1 a few milliseconds later (Figure 7.1). The electric potential is recorded in the (FDI) muscle contralateral to the motor cortex that received the test stimulus. This is called the Motor-Evoked Potential (MEP). The MEP after a pair of conditioning and test stimuli is compared to the MEP from a test stimulus alone (i.e., without conditioning stimulus). If the MEP with conditioning is lower than the MEP without conditioning stimulus, then the interhemispheric interaction between the opposing sites is said to be inhibitory. Interhemispeheric interactions are often quantified as the amplitude of conditioned MEP expressed as a percentage of the MEP from test stimulus alone. Values less than 100% would imply interhemispheric inhibition, while values greater than 100% would imply facilitation.

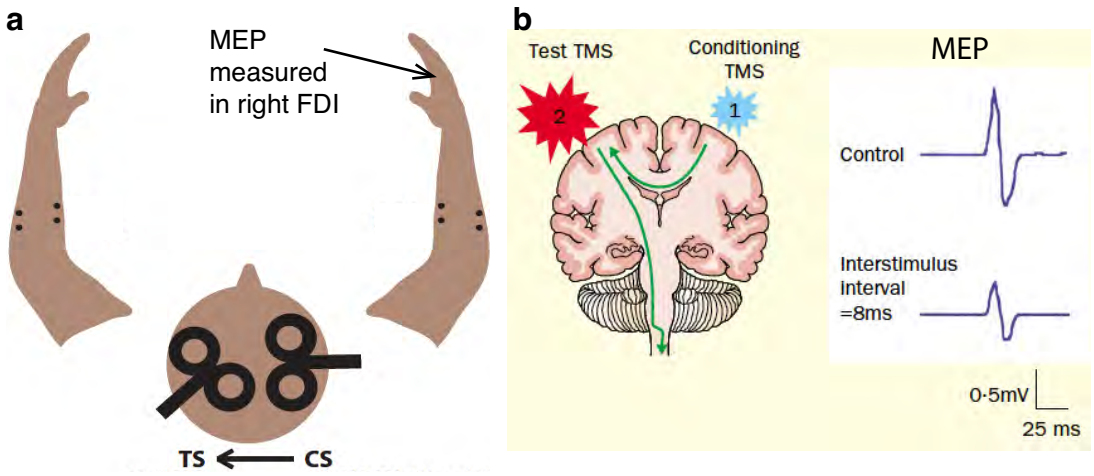

Figure 7.1: Interhemispheric inhibition measured using transcranial magnetic stimulation (TMS). **a**. A conditioning stimulus is sent to the right hand motor area, followed by a test stimulus to the left motor area a few milliseconds later. The motor evoked potential (MEP) is measured in the right FDI muscle, contralateral to the test stimulus. **b**. The measured MEP is compared to the control case where no conditioning stimulus was applied. The MEP amplitude is lower with conditioning (bottom trace) than without (top trace), which indicates interhemispheric inhibition (IHI) between left and right hand motor cortices. Figures adapted and modified from Ibey et al. (2015) and Kobayashi & Pascual-Leone (2003).

To understand the nature of interhemispheric inhibition with respect to contralateral activity, the conditioning stimulus can be changed to simulate varying amounts of activity in the contralateral M1. For example, Ni et. al. used a conditioning-test paradigm and measured First Dorsal Interosseous (FDI) muscle activation changes to explore interhemispheric inhibition (IHI) in the hand area of the primary motor cortex (Ni, Gunraj,

Nelson, Yeh, Castillo, Hoque & Chen 2009). The inhibition at the left M1 as a function of right M1 conditioning intensity followed a non-linear function resembling a sigmoid; it increased with conditioning stimulus intensity following a weak non-linearity (see Figure 7.2). Other studies have also shown non-linear inhibition at the primary motor cortices. For instance, Harris-Love et. al. and Morishita et. al. both found a similar non-linear relationship between conditioning stimulus intensity and amount of inhibition at the ipsilateral FDI muscle of the hand (Harris-Love, Perez, Chen & Cohen 2007, Morishita, Uehara & Funase 2012). Similarly, other hand or arm muscles also exhibited non-linear inhibition as a function of conditioning stimulus intensity; for example, wrist muscles (Flexor Digitorum Radialis and Extensor Digitorum Radialis Brevis) were investigated at different conditioning stimulus intensities and at different inter-stimulus intervals (ISI, i.e., the time interval between conditioning stimulus and test stimulus) (Ibey et al. 2015). The inhibition function was again non-linear.

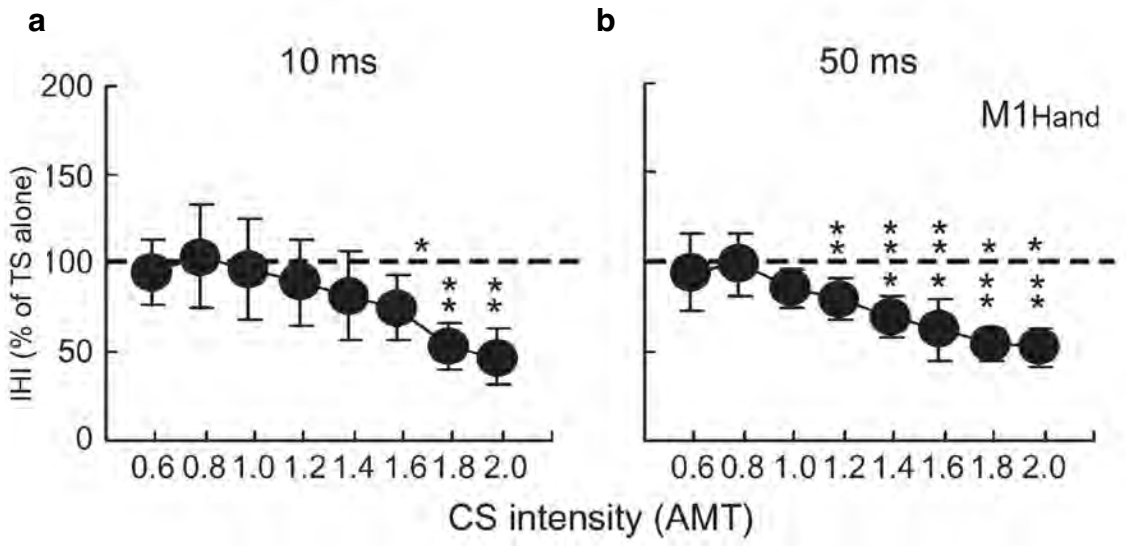

Figure 7.2: Interhemispheric inhibition as a function of conditioning intensity in the first dorsal interosseous (FDI) muscle (figure from Ni et al. (2009)). The conditioning stimulus (CS) was delivered to the right M1, and a test stimulus (TS) was delivered to the left M1. The MEP (motor-evoked potential) was measured in the right FDI muscle at different conditioning stimulus intensities (x-axis). The y-axis indicates the percent change in the amplitude of muscle activity compared to the control case with test stimulus alone (i.e. without conditioning). A decrease in %TS indicates inhibition. **a**. TS delivered 10 ms after CS, **b**. TS delivered 50 ms after CS.

Based on our previous experimental results indicating cortical involvement and left/right laterality in the production of goal-equivalent variability, as well as TMS studies investigating the nature of IHI in the hand M1, in this chapter, we develop a mathematical

model of interhemispheric inhibition as a mechanism to produce goal-equivalent variability. Our proposed model is a two-dimensional non-linear system of differential equations describing the amounts of activity in either M1 (left and right), where each M1 sends an inhibitory signal to the opposing side in the form of a sigmoid. A common input to both M1s is varied as an on/off repetition scheme representing a task similar to our experimental protocol in Chapter 4. This system belongs to the category of bistable systems, which comprise of non-linear differential equations with two distinct stable fixed points; and convergence to either is dictated by initial conditions (Morishita & Yajima 1972, Trotta, Bullinger & Sepulchre 2012). These types of systems have in common a non-linear feedback, and have been employed in modeling various types of biological phenomena, namely, genetic control (Griffith 1968), neural networks (Hopfield 1982, Myre & Woodward 1993), and species populations dynamics (Lotka 1925, Volterra & Brelot 1931).

We suggest that this mutually-inhibitory model with the addition of independent noise will allow for a spontaneous switching between the two stable states at different repetitions of the task. Moreover, we find that the shape of the mutual inhibition plays a role in making the output of the system reproduce our experimental results of goal-equivalent variability in output forces. Therefore, we explore the space of parameters that form the input and inhibition function, with the goal of defining conditions on the parameters that would result in valid solutions comparable to our experimental results.

7.2 Methods

Mutually-inhibiting bistable system

Inspired by a mutually-inhibiting neuronal model (Myre & Woodward 1993), we considered a system of two variables, x_L and x_R, representing the activity in left and right M1, respectively. There was common input to each x_L and x_R, and each M1 included linear self-inhibition, in addition to non-linear inhibition originating from the opposing M1. Figure 7.3 shows a sketch of the connections.

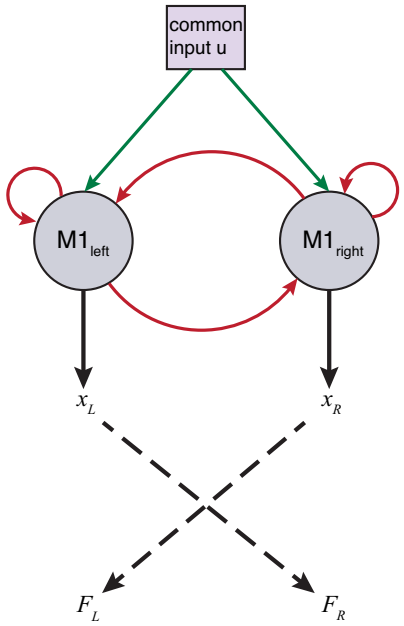

Figure 7.3: A sketch of the connections in the M1-M1 model. The colors represent the type of interaction: green implies an excitatory input, while red implies inhibition. There is a common input to both M1s, and mutual inhibition between the two. The activity at each M1 (x_L and x_R) would eventually produce force at the contralateral hand (F_R and F_L, respectively).

A linear mutual inhibition does not allow convergence to different solutions, because the system would have one stable fixed point, and therefore would always converge to the same solution. Therefore, we used non-linear functions to represent the mutual inhibition between x_L and x_R. We adapted a neural network model of two mutually-inhibiting neurons (Myre & Woodward 1993):

$$\begin{aligned} \frac{dx_L}{dt} &= -x_L - c\frac{1}{1+e^{-b(x_R-T)}} + u \\ \frac{dx_R}{dt} &= -x_R - c\frac{1}{1+e^{-b(x_L-T)}} + u \end{aligned} \tag{7.1}$$

Here, x_L and x_R represent the activity at the left and right M1s, respectively, u is the common input to both, b is a gain, T is a threshold and c is the strength of the inhibition. There is linear feedback from each x_i onto itself, and a non-linear feedback originating from the opposing x_j.

The non-linear inhibition $\frac{c}{1+e^{-b(x_i-T)}}$ is a sigmoid function of the activity of the opposing hemisphere. Figure 7.4 shows this nonlinearity as a function of x with parameters such that $c = 1, b = 5$ and $T = 0.5$. This feedback model was a plausible choice because interhemispheric inhibition in the hand area has been shown to exhibit a weak nonlinearity as a function of conditioning stimulus (Ni et al. 2009).

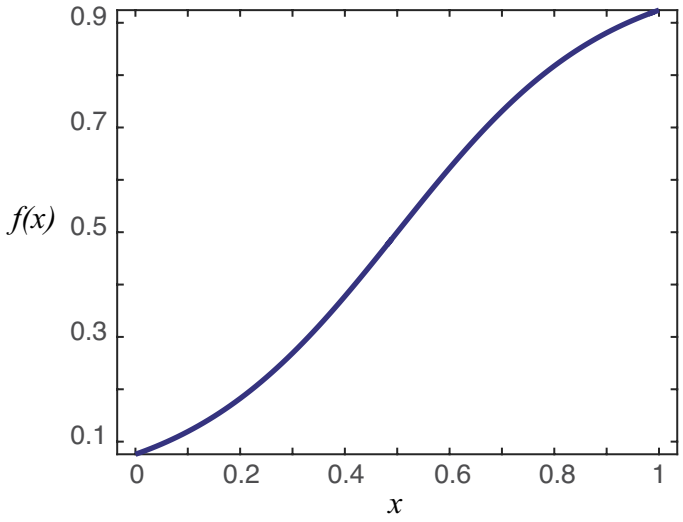

Figure 7.4: Sigmoid function $f(x) = \frac{c}{1+e^{-b(x-T)}}$ with $c = 1, b = 5$ and $T = 0.5$.

A bifurcation analysis was performed by (Myre & Woodward 1993). We include this analysis in Figure 7.5. Depending on the parameter set c, b, T and u, the system may either have one stable fixed point, or three fixed points: two distinct stable points and a saddle. In the latter case, initial conditions dictate which fixed point the system converges to.

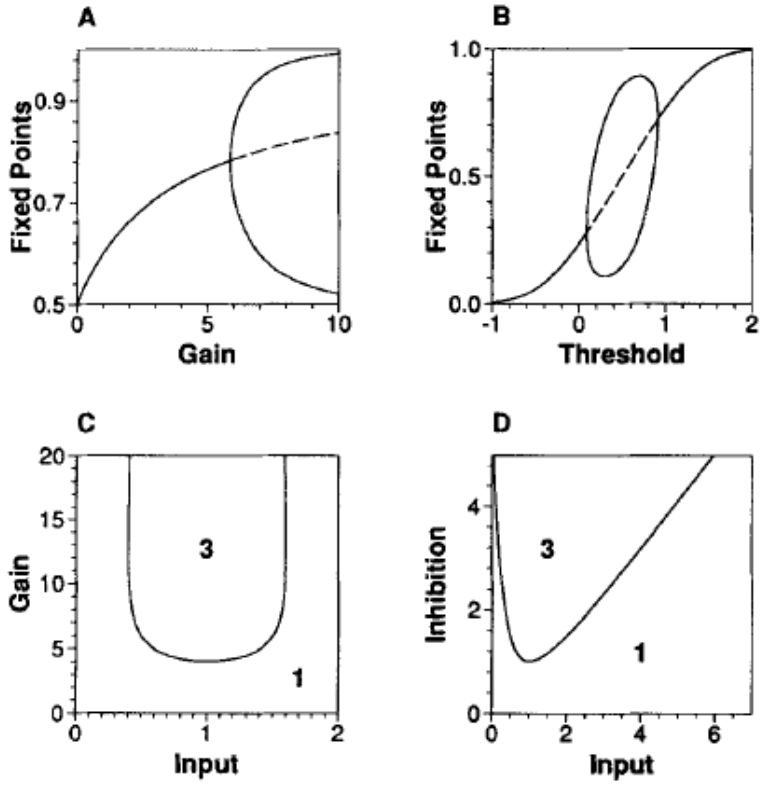

Figure 7.5: Bifurcation analysis. **A**. One of coordinates of the fixed point(s) of system (7.1) as a function of gain **b**. Continuous curves correspond to stable fixed points, dashed curves - to saddle fixed points ($T = 1$, $i = 1$, $c = 1$). **B**. The same as A but with varying the threshold T ($b = 5$, $i = 1$, $c = 1$). **C** and **D**. Bifurcation curves which separate the regions in parameter space corresponding to the system with one fixed point (denoted by **1**) from the regions corresponding to the systems with three fixed points (denoted by **3**). Parameter values are $T = 0.5$, $c = 1$ (for panel **C**); $T = 0.5$, $b = 4$ (for panel **D**). Figure and caption from (Myre & Woodward 1993).

For example, choosing $c = 1, b = 5, T = 0.5$ and $u = 1$ results in the phase plane in Figure 7.6. The two stable points of the system are $(0.145, 0.855)$ and $(0.855, 0.145)$. As

long as the initial conditions are such that $x_{0L} > x_{0R}$, the system converges to the stable point that has $x_L > x_R$, and vice-versa for $x_{0R} > x_{0L}$.

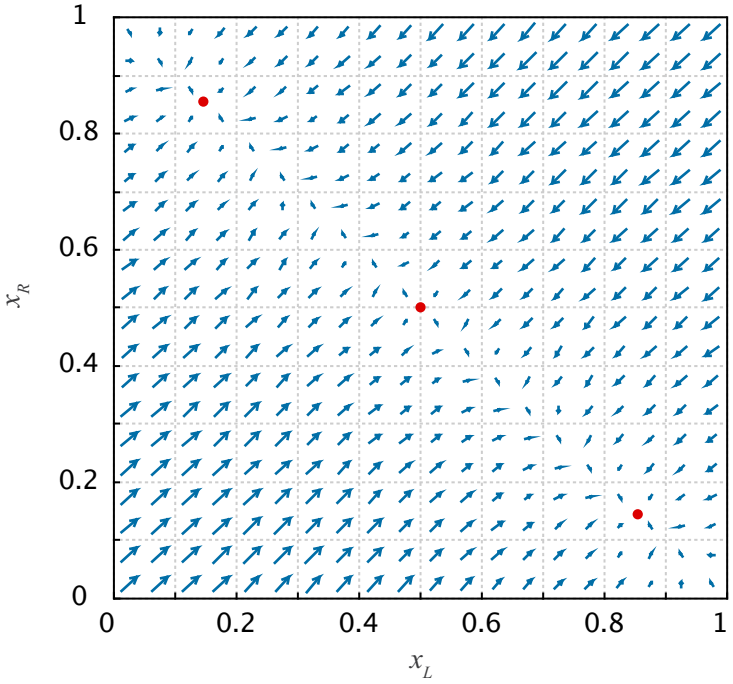

Figure 7.6: Phase-plane of the bistable system in (7.1) with $c = 1, b = 5, T = 0.5, u = 1$. The point in the middle is a saddle point $[(0.5, 0.5)]$, whereas the top left and bottom right points are the two stable states of the system $[(0.145, 0.855)$ and $(0.855, 0.145)]$.

As a summary, the system in (7.1) behaves the following way, depending on parameters and initial conditions:

1. if it has one stable fixed point, the solution always converges to this point.

2. if it is bistable (has two stable points and one saddle point such as in Figure 7.6):

   (a) for equal initial conditions, the solution always converges to the saddle point.

(b) for unequal initial conditions, the solution always converges to one of the two stable fixed points. If the initial conditions are such that $x_{0R} > x_{0L}$, then the system converges to the stable point corresponding to $x_R > x_L$, and vice-versa.

Therefore, repeated on/off inputs of u can not result in the spontaneous switch of the solution from $x_R > x_L$ to $x_L > x_R$ across repetitions (such as in Figure 4.1B) . As an example of a repeated input scheme representing repetitions of the target matching task, Figure 7.7 shows an on-time of 5 time points and an off-time of 4 time points (**a**). The system here eventually converged to $x_L = x_R$ (**b**).

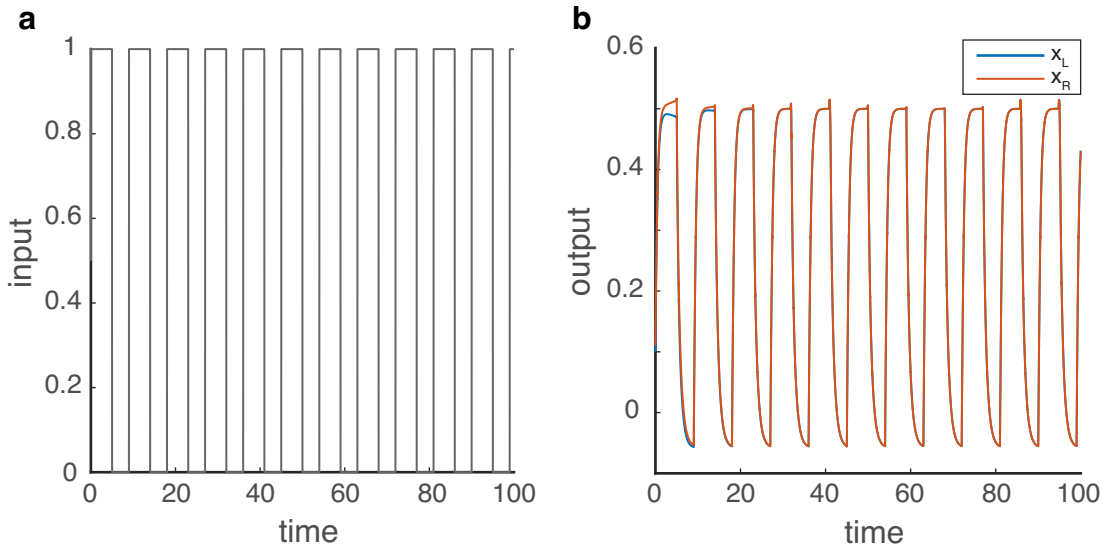

Figure 7.7: Example simulation of the system in 7.1 with repeated inputs. **a**. Input of the system with $u = 1$ for 5 time points and $u = 0$ for 4 time points. **b**. Output of the system, x_R and x_L, with initial conditions $x_{0L} = 0.1$ and $x_{0R} = 0.11$.

Adding noise

A well-studied aspect of neurons and neuronal activity is that neurons exhibit noise

even when tested under the same conditions. Variability in the neuronal activity is present in the primary motor cortex (Lee, Port, Kruse & Georgopoulos 1998), and tends to be correlated between neurons with high signal correlation (i.e., neurons that carry redundant messages). We therefore modified the system of equations in (7.1) to add independent random noise to each of x_L and x_R:

$$\begin{aligned} \frac{dx_L}{dt} &= -x_L - c\frac{1}{1+e^{-b(x_R-T)}} + u + \epsilon_1 \\ \frac{dx_R}{dt} &= -x_R - c\frac{1}{1+e^{-b(x_L-T)}} + u + \epsilon_2, \end{aligned} \tag{7.2}$$

where ϵ_1 and ϵ_2 are added random noise, each from a gaussian distribution with mean 0 and standard deviation σ: $\mathcal{N}(0, \sigma^2)$.

As an example of the system with added noise, we used the same input repetitions as in Figure 7.7 applied to the system in (7.2). Figure 7.8 shows the input and simulated output repetitions. In this case, the response exhibited a spontaneous switching between $x_R > x_L$ and $x_L > x_R$ (**b**).

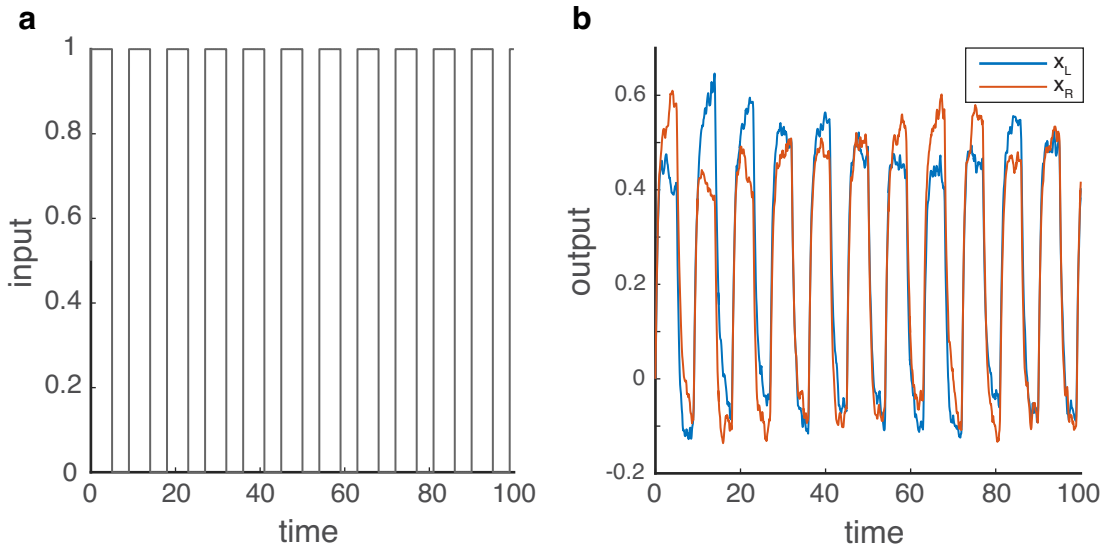

Figure 7.8: Example simulation of the system in 7.2 with repeated inputs including noise. **a**. Input of the system with $u = 1$ for 5 time points and $u = 0$ for 4 time points. **b**. Output of the system, x_R and x_L, with initial conditions $x_{0L} = x_{0R} = 0$.

Parameter space exploration

To understand the effects of the parameters on the inhibition function and the output of the system, we explored different combinations of parameters and simulated the system with repeated inputs (5 on, 4 off input repetition scheme for 200 time points). The free parameters are c, b, T, u and σ. We performed 1000 simulations where at each iteration the parameters were randomly selected from a uniform distribution with the intervals:

$c : [0, 5]$

$b : [0, 20]$

$T : [-1, 2]$

$u : [0, 7]$

$\sigma : [0, 0.2u]$ (upper limit of 20% of u)

These intervals were adapted from the bifurcation analysis that was performed in (Myre & Woodward 1993).

For each of the 1000 simulations we performed, we used the following criteria to decide if the output repetitions represented a valid solution comparable to our experimental results:

(i) the repetition means are non-negative;

(ii) the major axis of the fitted ellipse is approximately parallel to the line joining (0,1), (1,0);

(iii) the variance ratio > 0.8, as per our experimental results in Figure 4.2.

7.3 Results

An example simulation using the system of equations 7.2 was performed using the parameter values $c = 1$, $b = 4$, $T = 0.5$, $u = 1$, and $\sigma = 0.2$ in Figure 7.9. The input repetitions were "on" for 5 time points, and "off" for 4; and the simulation was run for 1000 s, yielding a total of 110 repetitions. Figure 7.2A shows a few of the simulated repetitions, indicating the sum of x_R and x_L was approximately constant at 1 across repetitions (top trace in black). The addition of noise allowed for individual activity to vary from repetition to repetition, resulting in some repetitions being achieved with $x_R > x_L$, and others with $x_L > x_R$ (bottom trace). We extracted (x_L, x_R) pairs averaged across each repetition, and show them in Figure 7.9B, where a 95% covariance ellipse was fit to

the data. The highest variation was observed across the major axis of the ellipse, where $x_R + x_L = 1$, while the lowest variation occurred across the minor axis.

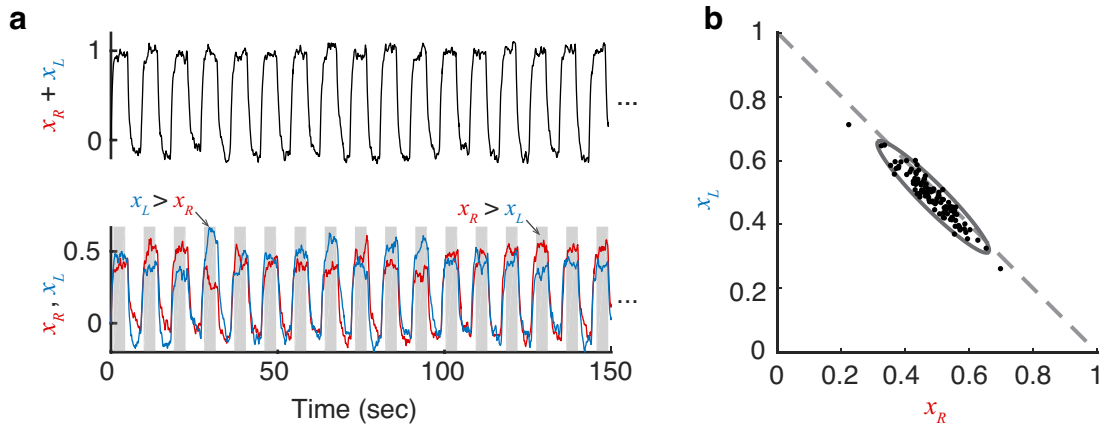

Figure 7.9: Example simulation and covariance ellipse with $c = 1$, $b = 4$, $T = 0.5$, $u = 1$, and $\sigma = 0.2$. **a**. a few of the simulated repetitions. The top trace shows $x_R + x_L$ maintained at 1 across repetitions; while the bottom traces show x_L (in blue) and x_R (in red) for the same repetitions. Some repetitions had a relatively higher right activity than left ($x_R > x_L$), and others vice-versa ($x_L > x_R$). The interval shaded in gray is used to determine the time average of individual activities in each repetition; **b**. average right versus left activities during all 110 repetitions with a 95% covariance ellipse representing the variance of the data. The major axis represents the goal-equivalent direction, where the sum of activities is always 1, while the minor axis is the non-goal-equivalent direction where the sum would deviate from 1. The highest variation is seen in the goal-equivalent direction, while the orthogonal non-goal-equivalent direction has much lower variance

Parameter space exploration

Figure 7.10a shows all 95% covariance ellipses from 1000 simulations that were performed with different parameter sets. Each ellipse was fit to the repetition means for each iteration. Figure 7.10b shows the 267 ellipses corresponding to simulations that were determined as being valid solutions based on the criteria listed in the Results section. All ellipses here have their major axes correspond to the goal-equivalent line where $x_R + x_L$ is always constant.

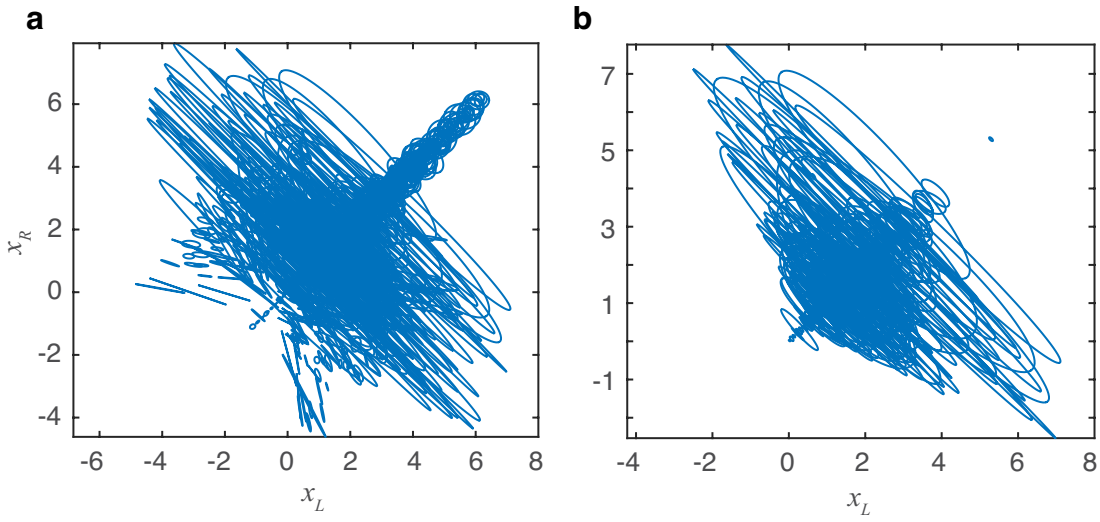

Figure 7.10: Covariance ellipses fit to each of 1000 simulations with randomly selected parameters. **a**. All ellipses superimposed, **b**. ellipses from valid parameter sets determined using the criteria mentioned in the text.

Valid inhibition functions

To understand the condition(s) that make the solution valid, we show all inhibition functions for the valid solutions $c\frac{1}{1+e^{-b(x_R-T)}}$ in Figure 7.11 (left), along with all inhibition functions for invalid solutions (right). The lines were color-coded based on the amplitude of u at each iteration. Some Inhibition functions for invalid solutions included linear functions, whereas all inhibition functions for valid solutions were non-linear. Moreover, for valid solutions, the amplitude of u appeared proportional to c, the scaling of the sigmoid, whereas no clear relationship was seen for invalid solutions. We show this relationship between c and the amplitude of u in Figure 7.12. In the valid set of solutions (left), u is proportional to c, whereas no clear relationship is seen in the set of invalid solutions (right).

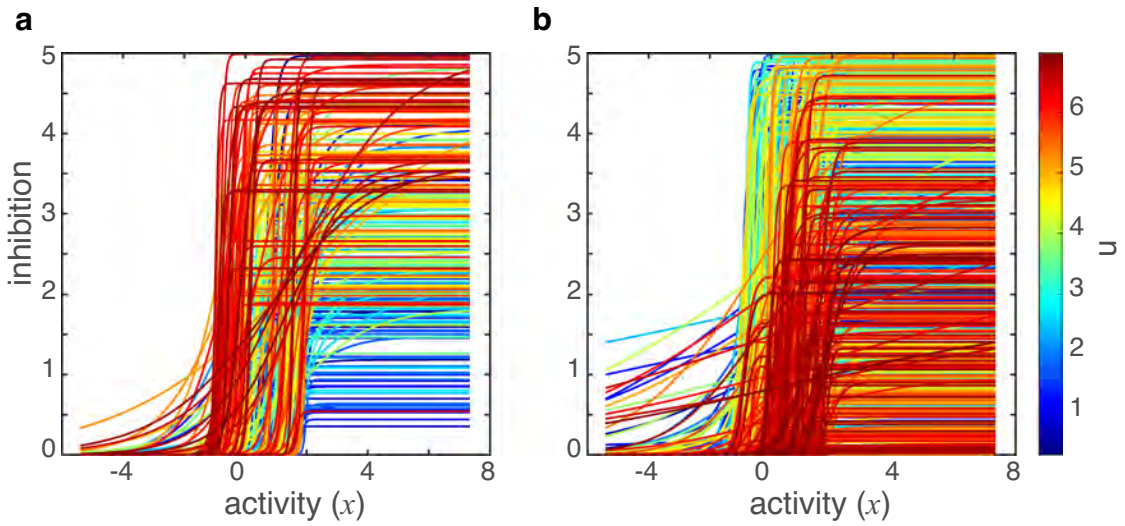

Figure 7.11: Inhibition functions of valid (**a**) and invalid (**b**) parameter sets. Each curve represents the inhibition function for one simulation, plotted against x using $\frac{c}{1+e^{-b(x-T)}}$ with the set of parameters c, b and T corresponding to that simulation. Each curve is colored with the amplitude of u for the corresponding simulation.

To further investigate the relationship between c and u in valid and invalid solutions, we performed simulations for fixed values of u. In other words, we ran a 1000 simulations, 7 times, where all parameters except for u were randomly selected at each iteration, while the amplitude of u was held constant at $u = 1, 2, 3, 4, 5, 6,$ or 7. The results are shown as box plots in Figure 7.13 for valid (**a**) and invalid (**b**) solution sets. In the valid solutions, there was a clear linear increase of c with the increase of u starting at $u = 2$, while invalid solutions did not show a relationship between c and u.

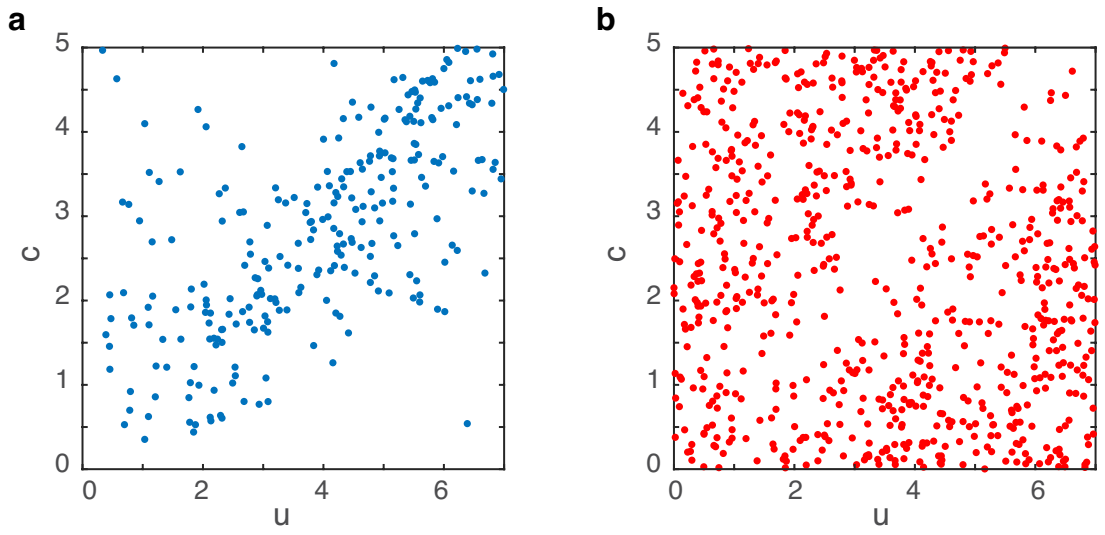

Figure 7.12: Relationship between inhibition scaling c and input amplitude u for valid (**a**) and invalid (**b**) parameter sets. 1000 simulations were carried out with randomly selected parameters each time. Valid parameter sets were selected according to the criteria described in the text. **a**. For valid parameter sets, the amplitude of u and the scaling of inhibition c followed a linear relationship. **b**. Invalid parameter sets did not exhibit any clear relationship between c and u.

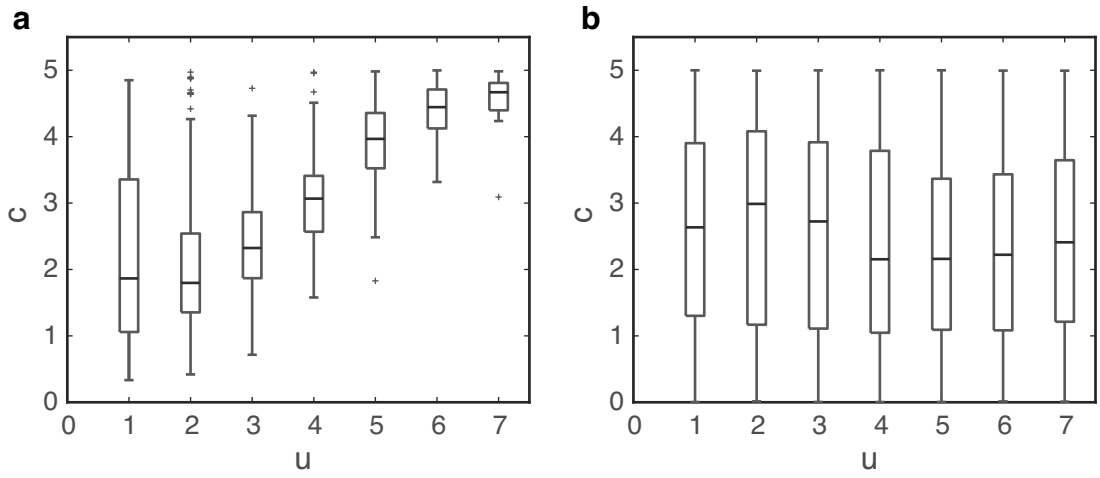

Figure 7.13: Boxplot showing the relationship between inhibition scaling c and input amplitude u for valid (**a**) and invalid (**b**) parameter sets. For each fixed u amplitude, 1000 simulations were carried out with the rest of the parameters randomly-selected from uniform distributions. Valid parameter sets were selected according to the criteria described in the text. **a**. The box plots of c with respect to u from valid parameter sets show a clear linear increase in c with respect to the amplitude of u. **b**. No clear relationship was observed between c and u for non-valid parameter sets.

7.4 Discussion

We observed a switching of the solution from $x_L > x_R$ to $x_R > x_L$ with the addition of noise to the bistable system in (7.1) (Figures 7.7 and 7.9). Moreover, the means across repetitions spanned an ellipse such that $x_R + x_L$ was constant throughout repetitions (Figure 7.9). We explored the space of parameters that define the system in (7.1) and identified the sets of parameters that agree with our experimental results of Figure 4.2.

We found that the inhibition function had an effect on the validity of the solutions. A non-linear inhibition function was not a sufficient condition for the solution to agree with our experimental results; rather, a linear relationship between c and u was required for the solution to be valid: the higher the input u, the higher scaling c of the inhibition was needed.

The non-linear nature of the inhibition function in our mathematical model agrees with interhemispheric inhibition functions investigated using TMS. These studies have shown a clear non-linearity of the inhibition with respect to increasing activity of the contralateral hemisphere (Ferbert et al. 1992, Ni et al. 2009). The inhibition functions were determined by delivering conditioning and test stimuli to the M1s, each time with a different conditioning stimulus intensity representing contralateral activity. As the intensity of the conditioning stimulus on one hemisphere was increased, the inhibition at the contralateral hemisphere where a test stimulus was delivered also increased. In the hand area and in particular the FDI muscle, the increase in inhibition with respect to increasing conditioning stimulus intensity was found to be non-linear, often resembling a sigmoid (Chen, Yung & Li 2003, Ni et al. 2009, Fling & Seidler 2012, Harris-Love et al. 2007, Morishita et al. 2012).

Our simulations with different parameter sets revealed that the non-linearity of the inhibition function was not enough for the system to replicate our experimental results of goal-equivalent variability of force output. In addition to having a sigmoidal shape, the amplitude of the inhibition function for valid solutions scaled with the amplitude of the input u. To our knowledge, this result has not been shown using TMS. We suggest further TMS experiments with a conditioning-test paradigm while participants perform

the bimanual goal-equivalent finger force task as in Chapter 4, with a few different target levels. During repetitions, a conditioning stimulus would be sent to the FDI hot-spot of the right M1, with a test stimulus at the left M1 following a few ms after. The MEP would be measured in the right FDI following the test stimulus and compared to the MEP without conditioning. This paradigm would be repeated using higher conditioning stimulus intensities; and the inhibition function would be determined with respect to conditioning stimulus intensity. The same steps would be taken to determine the inhibition function at different force target levels, representing a scaling of u. The inhibition functions at different target levels would be compared to determine if the scaling of the inhibition, representing c, increases with u in agreement with our simulation results.